Magnitude Scaling of Free Surface Depression during High Current Arc Welding

P.F. Mendez, T.W. Eagar

Massachusetts Institute of Technology, Cambridge, MA

Proceedings of the 5th International Conference Trends in Welding Research, June 1-5, 1998, Pine Mountain, GA, pp 13-18.

Abstract

Arc welding at high current and speed presents some unique characteristics and problems. Perhaps the most noticeable of these characteristics is the large depression created under the arc, which in some cases resembles "dry" metal. Many authors have associated this large depression with the presence of defects such as undercutting, humping and tunnel porosity[1-5]. In this work, we apply a dimensional scaling method developed at the Welding and Joining group at MIT[6] to GTA welding at high currents. At high current and welding speed the shear force of the plasma on the free surface determines the flow of liquid metal under the arc. This causes the weld pool under the arc to turn into a thin liquid film. In this situation, the arc force acts almost directly over the melting interface, causing a deep weld penetration and a potentially unstable liquid film.

Introduction

Welding has very important economic implications; approximately 500 million tons of product are welded each year in the world, using about $6 billion of welding consumables. Since welding is performed relatively late in the manufacturing process, a defective weld can cause the loss of the value added by all of the preceding production stages.

In order to increase welding productivity, the welding speed and the current are constantly increased. This strategy is limited by the appearance of defects, typically: humping, undercutting and tunnel porosity[3,5]. Figures 1-3 show the details of a humped weld bead. Many authors have associated these defects with the deep weld pool surface depression observed during high current arc welding[1-5], Most speculations about penetration at high currents have been related to the action of the arc over the "dry" metal[3,7-10].

One of the difficulties in the study of deeply depressed weld pools at high currents is that the relative order of magnitude of the driving forces is unknown. With higher currents, the electromagnetic forces increase, but the weld pool geometry also changes. Thus, the relative effect of these forces is unknown. Ishizaki[7] proposed that the plasma arc pushes the weld pool to the rear. Choo *et al.*[11] suggested that at high current levels the gas shear on the free surface could be as important as the Marangoni forces. Experiments and calculations done by Lin and Eagar[4], and Rokhlin and Guu[12] showed that at currents over 300A, the free surface depression is about five times the value obtained from surface energy minimization under arc pressure alone. Therefore electromagnetic and hydrodynamic forces must be taken into account.

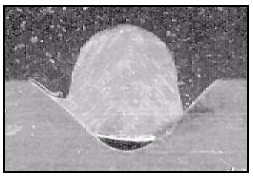

Figure 1: Cross section A-A

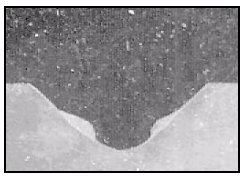

Figure 2: Cross section B-B

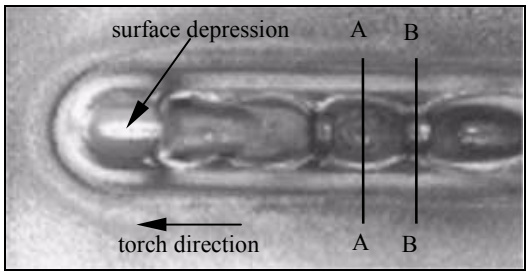

Figure 3: Top view

Another obstacle in the study of high current welding is that a numerical solution to the problem becomes more difficult as the curvatures and slopes increase. Most published analyses of the weld pool consider a flat or moderate free surface deformation in which recirculating flows under the arc still exist. Also, the non-linearity of the Navier-Stokes equations does not guarantee a unique solution, especially when the position of the free surface is also considered an unknown. Lin and Eagar[13] reported the existence of a hysteresis cycle in GTA in which two different values of penetration are possible for the same welding settings, depending upon whether the current was increasing or decreasing.

Because analytic solutions do not present the stability problems of numerical solutions, many attempts have been made at solving the problem analytically or estimating the magnitude of the solutions (scaling). Some scaling factors were obtained by Oreper and Szekely[14], Thompson and Szekely[15], and Rivas and Ostrach[16] for weld pools with moderately deformed free surface (i.e. with recirculating flows under

the arc). These three works consider Marangoni as the dominant force in the molten metal.

In this work, we perform a magnitude scaling of the weld pool under a high current arc considering gas shear, arc pressure, and various forces acting on the molten metal including Marangoni, capillary, electromagnetic, gravity and buoyancy. This magnitude scaling method builds upon the general knowledge we have about the solution of a problem. It provides an estimation of the value of the unknowns in the problem and weighs the importance of each of the driving forces mentioned above. All of this information is obtained without the need to solve the set of partial differential equations. Since the scaling factors obtained have algebraic expressions, they can be used subsequently with different materials and situations. These scaling factors can only be considered as an approximation; when an accurate result is necessary, the coupled system of partial differential equations must be solved or sufficient experiments must be performed.

Overview of the Problem

Figure 4 shows schematically a side view of the weld pool under a high current arc. If we consider that the welding torch is stationary, the substrate moves to the right with velocity U_∞. If we consider that the substrate is stationary the torch moves to the left, leaving a trail of solidifying metal. The weld pool has two characteristic regions, one is very thin and occurs under the arc (usually considered "dry"), and the trailing part which is thicker. In this work we are going to concentrate on the front end of the weld pool.

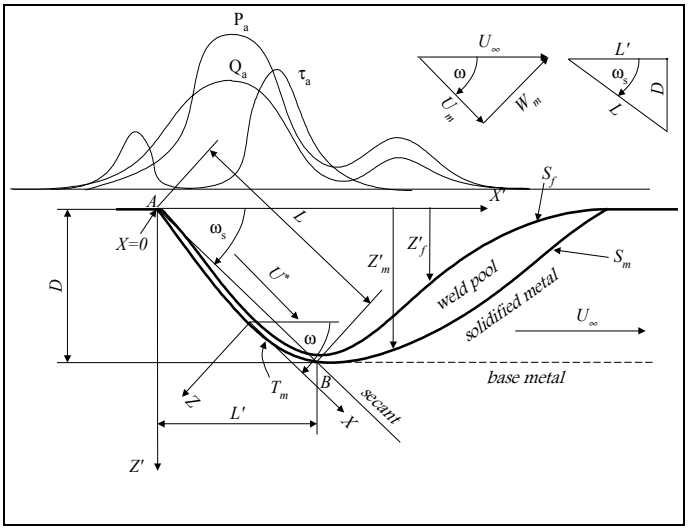

Figure 4: Schematic of a thin weld pool under the action of a high current arc

The curves labeled Q_a, P_a, and τ_a represent the heat input, arc pressure, and shear stress that the arc imposes on the free surface. To the best of our knowledge no studies have been performed to determine the exact shape of these curves for deeply depressed weld pools. S_f and S_m represent the free surface and the melting interface (assuming that the base metal has a sharp melting point). In this problem we will consider S_m as prescribed, and S_f as an unknown to be determined.

For simplicity, we consider a two-dimensional problem, neglecting transport phenomena along the Y axis. The reference axes travel with the welding torch so that the problem can be solved as a pseudo-stationary one. The axes X and Z are tangential and normal to the melting interface (S_m), therefore their angle ω with the horizontal (X') changes along the melting front. We can neglect the derivatives with respect to ω when using the scaling relationships because the thickness of the liquid film is much smaller than the radius of curvature of the melting front. This approach is very similar to the one used by Wei and Giedt in their study of keyhole formation in electron beam welding[17]. The melting front angle ω_s is the angle of a secant to the melting front between the point of beginning of melting (point A in Figure 4) and the point where maximum penetration is reached (point B).

Two-dimensional Analysis of a Thin Weld Pool

Arc behavior

In the absence of specific data for deeply depressed weld pools, it is necessary to make some assumptions about the characteristics of the arc. The starting points are the measurements by Tsai[18] and modeling by Choo[19] for flat free surfaces. The heat distribution between the front and rear of the weld pool is unknown. It is reasonable to assume that most of the heat is delivered to the melting front because it is closer to the electrode. A smaller fraction of the power heats the tail end. Due to the deep depression, the arc length is somewhat longer than it is for a flat plate, and can be approximated as:

$$\text{arc length} \approx \text{arc length}_{\text{flat}} + D/2 \tag{1}$$

The arc acts over a larger area on the melting front than on a flat surface. Its maximum parameters can be estimated as:

$$Q_{\max} \approx Q_{\max,\,flat}\cos(\omega_s) \tag{2}$$
$$P_{\max} \approx P_{\max,\,flat}\cos(\omega_s) \tag{3}$$
$$J_{\max} \approx J_{\max,\,flat}\cos(\omega_s) \tag{4}$$
$$\tau_{\max} \approx \tau_{\max,\,flat} \tag{5}$$

These approximations are conservative because they underestimate the importance of the dominant driving force, and overestimate the magnitude of the other forces. The gas shear stress over the surface is expected to be larger than over a flat surface because of the slope of the melting front the weld pool. On the other hand, since a fraction of the arc energy is diverted to the tail, the maximum heat input and current (and perhaps pressure) are expected to be even smaller than these estimations. Surface heat losses under the arc are not considered because they are of the order of the uncertainty in the arc estimations.

Scaling relationships

The following scaling relationships convert the dimensional equations into their non-dimensional counterparts.

$$X = Lx \tag{6}$$
$$X' = L'x' \tag{7}$$
$$Z = \delta^* z \tag{8}$$
$$\delta(X) = \delta^* \Delta(x) \tag{9}$$
$$U(X,Z) = U_m(\omega) + U^* u(x,z) \tag{10}$$
$$W(X,Z) = W_m(\omega) + W^* w(x,z) \tag{11}$$
$$P(X,Z) = P^* p(x,z) \tag{12}$$
$$T(X,Z) = T_m + T^* \theta(x,z) \tag{13}$$
$$Z_f(X') = D\, z_f(x') \tag{14}$$

$$Z_m(X') = D\, z_m(x') \quad (15)$$

$$\mathrm{Q_a}(X) = Q_{\max}\, \mathrm{q}_a(x) \quad (16)$$

$$\mathrm{P_a}(X) = P_{\max}\, \mathrm{p}_a(x) \quad (17)$$

$$\tau_a(X) = \tau_{\max}\, \mathrm{t}_a(x) \quad (18)$$

$$\mathrm{J_a}(X) = J_{\max}\, \mathrm{j}_a(x) \quad (19)$$

$$J_x(X,Z) = J^*\, j_x(x,z) \quad (20)$$

$$J_z(X,Z) = J_{\max} j_z(x,z) \quad (21)$$

$$B_y(X,Z) = B^*\, b(x,z) \quad (22)$$

$$\Phi(X,Z) = \Phi^*\varphi(x,z) \quad (23)$$

where:

$$U_m(\omega) = U_\infty \cos(\omega) \quad (24)$$

$$W_m(\omega) = -U_\infty \sin(\omega) \quad (25)$$

Table I: Exponents of the physical magnitudes in the scaling parameters

	L	k	Q_{max}	J_{max}	σ_e	μ	C_1'	τ_{max}	μ_0	U_∞
δ^*	0.5					0.5	-0.5	-0.5		0.5
U^*	0.5					-0.5	-0.5	0.5		0.5
W^*							-1			1
P^*	0.5					-0.5	0.5	1.5		-0.5
T^*	0.5	-1	1			0.5	-0.5	-0.5		0.5
Φ^*	0.5			1	-1	0.5	-0.5	-0.5		0.5
J_x^*	-0.5			1		0.5	-0.5	-0.5		0.5
B^*	1			1					1	

In Table I and Table III the value of C_1' is:

$$C_1' = C_1/\sin(\omega_s) \quad (26)$$

Non-dimensional system of equations

The following expressions were obtained by performing a magnitude scaling of the original equations for a two-dimensional, pseudo-stationary system. Implicit in these equations is that the dominant driving force for the fluid flow is the gas shear at the surface. This assumption does not affect the generality of the mathematical formulation, but it allows the unknown scaling parameters to be of the order of the functions they scale.

Eq. 27 is the equation of continuity, Eqs. 28-29 are Navier-Stokes, Eq. 30 is the equation of energy, and Eqs. 31-35 relate to the electromagnetic forces. In this two-dimensional system, the magnetic flux vector is perpendicular to the page at all times. Eq. 36 is an integral form of the mass conservation equation; it is not actually an equation, but an approximation, and is valid only when the weld pool thickness under the arc is much smaller than the weld penetration. Eqs. 37,39 relate to the forces the plasma and surface tension exert on the free surface; the former is the gas shear stress boundary condition (which includes Marangoni), and the latter is the pressure balance. Eq. 38 is the velocity in Z boundary condition at the free surface. Eqs. 40-41 relate to the heat and current fluxes from the arc on the free surface. Eqs. 42-44 are the velocity and pressure boundary conditions at the melting interface.

$$\frac{\partial u}{\partial x} + \frac{\partial w}{\partial z} = 0 \quad (27)$$

$$\Pi_1\left[(u+u_m)\frac{\partial u}{\partial x} + (w+w_m)\frac{\partial u}{\partial z}\right] = -\frac{\partial p}{\partial x} + \Pi_3\frac{\partial^2 u}{\partial x^2} + \frac{\partial^2 u}{\partial z^2} - \quad (28)$$
$$-\Pi_4\sin(\omega) - \Pi_5\, \mathrm{j_z b} - \Pi_6\sin(\omega)\theta$$

$$\Pi_1\Pi_3\left[(u+u_m)\frac{\partial w}{\partial x} + (w+w_m)\frac{\partial w}{\partial z}\right] = -\frac{\partial p}{\partial z} + \Pi_3\left(\Pi_3\frac{\partial^2 u}{\partial x^2} + \frac{\partial^2 u}{\partial z^2}\right) + \quad (29)$$
$$+\Pi_3^{1/2}\Pi_4\cos(\omega) + \Pi_3\Pi_5\, \mathrm{j_x b} - \Pi_3^{1/2}\Pi_6\cos(\omega)\theta$$

$$\Pi_7\left[(u+u_m)\frac{\partial \theta}{\partial x} + (w+w_m)\frac{\partial \theta}{\partial z}\right] = \Pi_3\frac{\partial^2\theta}{\partial x^2} + \frac{\partial^2\theta}{\partial z^2} \quad (30)$$

$$\mathrm{j_x} = -\frac{\partial \varphi}{\partial x} \quad (31)$$

$$\mathrm{j_z} = -\frac{\partial \varphi}{\partial z} \quad (32)$$

$$\Pi_3\frac{\partial^2\varphi}{\partial x^2} + \frac{\partial^2\varphi}{\partial z^2} = 0 \quad (33)$$

$$\frac{\partial \mathrm{b}}{\partial \mathrm{x}} = \mathrm{j_z} \quad (34)$$

$$\frac{\partial \mathrm{b}}{\partial \mathrm{z}} = -\Pi_3\, \mathrm{j_x} \quad (35)$$

$$1 + \frac{\Pi_3^{1/2}}{\sin(\Pi_2)} \approx 1 \quad (36)$$

Table II: Boundary conditions for a thin weld pool

	u	w	p	θ	φ	Δ	b
S_f	Eq. 37	Eq. 38	Eq. 39	Eq. 40	Eq. 14		
S_m	u_m	w_m	Eq. 44	0			
$x = 0$						0	
$x' = \pm\infty$					0		0
$z' = +\infty$					0		0

$$\frac{\partial u}{\partial z}\sqrt{1+\Pi_3\left(\frac{d\Delta}{dx}\right)^2} = -\mathrm{t}_a - \Pi_8\left(\frac{\partial\theta}{\partial x} + \frac{d\Delta}{dx}\frac{\partial\theta}{\partial z}\right) \quad (37)$$

$$w = \frac{\Pi_3^{1/2}}{\tan(\Pi_2)}(u+u_m)\Delta - w_m \quad (38)$$

$$p = \Pi_9\frac{\tan(\Pi_2)}{\left(1+\tan^2(\Pi_2)\left(\frac{dz_f'}{dx'}\right)^2\right)^{3/2}\cos(\Pi_2)}\frac{d^2 z_f'}{dx'^2} + \Pi_{10}\,\mathrm{p_a} \quad (39)$$

$$\frac{\partial\theta}{\partial z} = -\mathrm{q_a} \quad (40)$$

$$\frac{\partial\varphi}{\partial z} = -\mathrm{j_a} \quad (41)$$

$$u_m = \frac{\Pi_3^{1/2}C_1}{\sin(\Pi_2)}\cos(\omega) \quad (42)$$

$$w_m = -\frac{C_1}{\sin(\Pi_2)}\sin(\omega) \quad (43)$$

$$p = \Pi_4\sin(\Pi_2)z_m' \quad (44)$$

Eqs. 27-44 completely describe the problem, and are a function of ten Buckingham's parameters $\Pi_1 \ldots \Pi_{10}$, the constant C_1, and the angle ω. This angle describes the slope at each point of the melting front. The constant C_1 represents the ratio between the average velocity and the free surface velocity for the liquid film at point B (Figure 4). Its value is ½ for a totally viscous flow increasing to 1 for a uniform

velocity flow. We adopted $C_1 = ½$ because in a thin weld pool the flow is dominated by viscous forces.

For the two-dimensional system of equations presented above, the only simplifications made are to neglect the derivatives with respect to ω, and to neglect one of the terms in Eq. 10. In physical terms, the first of these simplifications means to consider the liquid film thickness as much smaller than the radius of curvature of the melting front, thus the angle ω can be considered constant point by point. The second simplification means that the flow in the film is much faster than the welding velocity. Physical simplifications are to consider the material as having constant thermophysical properties and a melting point like a pure metal.

The Π parameters have the form of a product of factors raised to a power. Table III shows the corresponding set of exponents.

Table III: Exponent of the physical magnitudes in dimensionless groups

	L	ρ	α	k	Q_{max}	J_{max}	g	ν	σ_T	σ	C_1'	P_{max}	τ_{max}	U_∞	μ_0	β	ω
Π_1	0.5	0.5						-0.5			-1.5	0	-0.5	1.5			
Π_2																	1
Π_3	-1	1						1			-1		-1	1			
Π_4	0.5	1.5					1	0.5			-0.5		-1.5	0.5			
Π_5	1.5	0.5				2		0.5			-0.5		-1.5	0.5	1		
Π_6	1	2		-1	1		1	1			-1		-2	1		1	
Π_7	0.5	0.5	-1					0.5			-1.5		-0.5	1.5			
Π_8	-0.5	0.5		-1	1			0.5	1		-0.5		-1.5	0.5			
Π_9	-1.5	0.5						0.5		1	-0.5		-1.5	0.5			
Π_{10}	-0.5	0.5						0.5			-0.5	1	-1.5	0.5			

All of the Π parameters have a concrete physical meaning, and many can be associated with well known dimensionless groups, as shown in Table IV. The parameters Π_4, Π_5, Π_6, Π_8, Π_9, and Π_{10}, are ratios of driving forces for the flow. The groups Π_1, Π_3, and Π_7, are ratios of effects. Π_2 relates to the geometry. The term "diffusivity" used to describe Π_3 refers to diffusion-like processes such as heat conduction or momentum transfer.

Table IV: Dimensionless parameters and their meaning

	physical meaning	*related group*[20]
Π_1	inertia/viscous	Reynolds
Π_2	melting front angle	ω_s in Figure 4
Π_3	diffusivity in x/diffusivity in z	
Π_4	gravity/viscous	Stokes
Π_5	electromagnetic/viscous	Elsasser
Π_6	buoyancy/viscous	Grashoff
Π_7	convection/conduction	Peclet
Π_8	Marangoni/viscous	Marangoni
Π_9	capillary/viscous	Capillary
Π_{10}	arc pressure/viscous	Poiseuille

One advantage of the system of Π numbers proposed here is that the ratios mentioned actually describe the relative orders of magnitude of driving forces or effects with more accuracy than the standard parameters. The reason for this is that they include information about the geometry and magnitudes of the problem that are not easily captured in traditional dimensional analysis.

Values for a typical case

For the evaluation of the relative importance of all the driving forces in the problem, we can focus on a typical weld with a deeply depressed surface. Images of this weld and its main welding parameters are shown in Figures 1-3 and Table V. The measured weld penetration and its location are:

$D = 3.2$ mm
$L' = 4.15$ mm
$\omega_s = 0.657$ rad

Table V: Welding parameters for weld of Figures 1-3

base material	AISI 304 (50 ppm S)
current	305 A
voltage	14.5 V
speed	12 ipm (5.08 mm/s)
arc length$_{flat}$	3.175 mm
shielding gas	100% Ar

With these settings, the estimated parameters for the arc are:

$Q_{max} = 3.34\ 10^7$ W/m^2
$P_{max} = 713$ Pa
$J_{max} = 4.29\ 10^6$ A/m^2
$\tau_{max} = 92.1$ Pa

Table VI: Physical properties for AISI 304 with 50 ppm S

ρ	6907	kg/m^3	ν	8.32 10^{-7}	m^2/s
α	3.30 10^{-6}	m^2/s	σ_T	1.50 10^{-4}	N/mK
k	18.0	W/mK	σ	1.56	N/m
σ_e	7.7 10^5	A/Vm	β	9.79 10^{-5}	1/K
T_s	1523	K	T_l	1723	K

Results

The scaling parameters obtained are presented in Table VII. The characteristic thickness for the liquid film is on the order of tens of microns, which is orders of magnitude smaller than the thickness for a weld pool with recirculation (of the order of millimeters). On such a thin weld pool, the characteristic temperature variation is of the order of 10^2 K, much smaller than that for weld pools with recirculation (of the order of 10^3 K). This smaller temperature jump makes Marangoni forces less relevant. Thus, variations in the sulfur content are expected to have a much smaller influence on penetration than in thicker weld pools.

Table VII: Values for the scaling parameters

δ^*	4.51 10^{-5} m	T^*	83.8 K
U^*	0.722 m/s	Φ^*	2.51 10^{-4} V
W^*	6.20 10^{-3} m/s	J^*	3.69 10^4 A/m^2
P^*	1.07 10^4 Pa	B^*	2.83 10^{-2} Wb/m^2

The values for the Π parameters are represented in Figure 5. The value 1 corresponds to the ratio between the viscous forces and the gas shear force (dominant). An analysis of the groups related to the driving forces shows that their influence is smaller than 10% of the dominant force. The very small value of Π_3 indicates that in the X-direction thermal conduction and viscous effects are negligible. Convection (Π_7) is very small, but inertial forces (Π_1) could be of importance.

The thickness of the mushy zone can be estimated as:

$$\text{thickness mushy zone} \approx k\,T_{sl}/Q_{max} = 1.07\,10^{-4}\,\text{m} \qquad (45)$$

The film thickness is only a half of this, and will capture the irregularities in the melting of the base metal, thus giving the impression of a "dry" surface.

The time scale in which the thin film would freeze is:

$$\text{time scale for freezing} = k\,T^*\delta^* \big/ \left(2\alpha Q_{\max}\right) = 3.1\ 10^{-4}\,\text{s} \qquad (46)$$

This time scale is much smaller than the arc residence time (of the order of 1 s), therefore the temperature of the weld is related directly to the heat input from the arc. When the arc extinguishes, the portion of the weld pool under the arc solidifies immediately, preserving the shape of the depression. If the thin film solidifies before reaching the tail of the weld pool, the fluid flow would be blocked and could not feed the tail (Figure 6b). The accumulation of liquid in front of the blockage is a potential cause for humping (Figure 6c). Giving the torch a leading angle would decrease the gas shear on the surface, thus producing a thicker and hotter film, which results in a longer time scale for freezing. This could explain the observations of Bradstreet[5], and Shimada[2] of a beneficial effect of leading torch angle on humped welds.

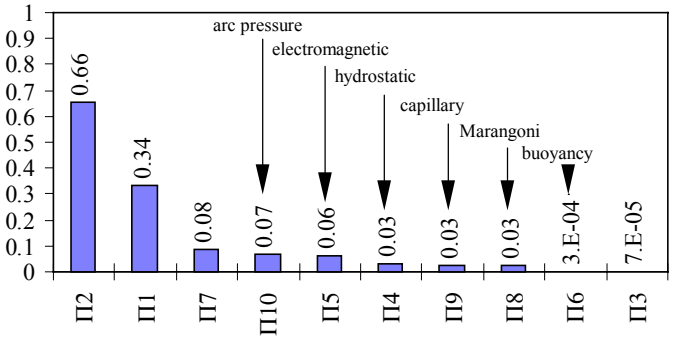

Figure 5: Magnitude of the Π parameters for a typical weld with large surface depression

Discussion

The non-dimensional system of equations Eqs. 27-44 considers that the layer thickness is much smaller than the radius of curvature of the melting front, and that one of the terms in Eq. 36 is negligible. Based on the results obtained above we can estimate these simplifications to be accurate of the order of 10^{-2}.

As mentioned above, the behavior of the arc in such a deeply depressed weld pool is not well known. It is difficult to estimate the tail end temperature and characteristics without knowledge of how much heat it receives. When the tail receives little energy, there is a risk of premature freezing of the thin film and humping with the mechanism described above. When the fraction of power reaching the tail is higher, temperature differences could be of the order of 10^3 K. In this case Marangoni forces are dominant and would produce strong recirculating flows. Ishizaki[8] suggested that this hot metal widens the weld bead after the arc acted over the melting front ("primary" and "secondary" penetration in his terms). Finger-like penetration in GTA welding can then be explained as a combination of a deep penetration caused by the direct action of the arc on the melting front, and a widening of the bead at the surface by the hot liquid of the tail (Figure 6a). For very fast welds, the tail can be very elongated and experience humping through a mechanism of capillary instabilities[21].

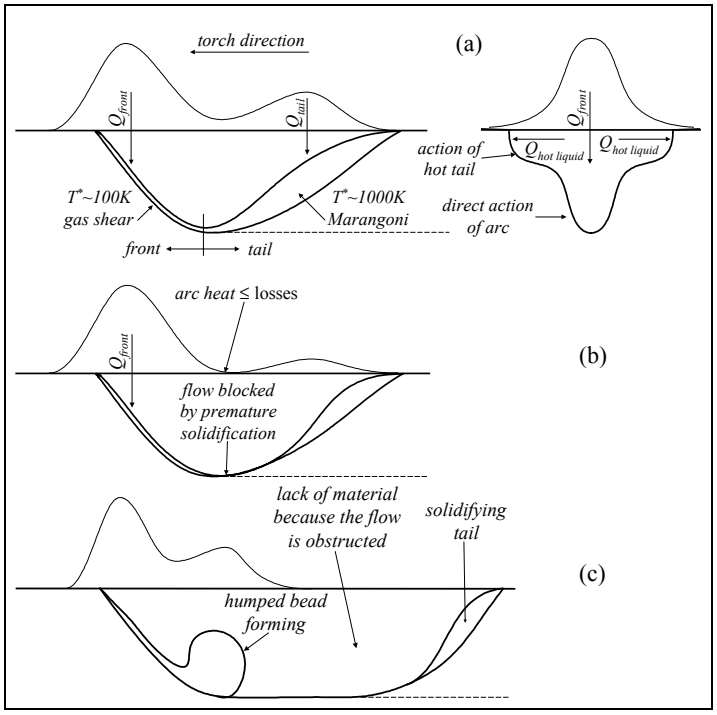

Figure 6: Schematic of finger-like penetration and humping formation in GTA welding

Conclusions

For thin weld pools under high current arcs, the gas shear stress is the main determinant of the motion of the liquid under the arc. Other factors such as Marangoni, electromagnetic and buoyancy have a much smaller effect.

The characteristic thickness, surface velocity and temperature under the arc can be evaluated with the following expressions (typical values are in parenthesis):

$$\delta^* = \left(2\mu U_\infty D/\tau_{\max}\right)^{1/2} \quad (\approx 50\ \mu\text{m}) \qquad (47)$$

$$T^* = Q_{\max}\delta^*/k \quad (\approx 100\ \text{K}) \qquad (48)$$

$$U^* = 2U_\infty D/\delta^* \quad (\approx 1\ \text{m/s}) \qquad (49)$$

The freezing time for the thin film is very small, and premature freezing can start a humped bead. A leading torch angle causes a thicker and hotter film with a longer time scale for freezing, which is helpful for humping problems.

The thickness of the weld pool is of the order of the mushy zone, therefore the free surface captures its irregularities and has the appearance of "dry" metal.

Finger-like penetration in GTA welding can be explained as a combination of the deep penetration caused by the direct action of the arc on the melting front, and a widening of the bead by the hot metal of the tail (Figure 6a).

A more accurate estimation of the characteristics of the arc in deeply depressed weld pools is necessary. This is especially important if the melting front is also considered an unknown, because the arc acts almost directly over it.

Acknowledgment

This work was supported by the United States Department of Energy, Office of Basic Energy Sciences.

List of Symbols

b	dimensionless magnetic flux
B^*	characteristic magnetic flux
B_y	magnetic flux
C_1	mass conservation constant
D	weld penetration
g	gravity
J^*	characteristic current density
ja	dimensionless current density at the surface
Ja	current density at the surface
J_{max}	maximum current density at the surface
j_x	dimensionless current density in x
J_x	current density in X
j_z	dimensionless current density in z
J_z	current density in Z
k	liquid heat conductivity
L	characteristic length in X
L'	characteristic length in X'
p	dimensionless pressure
P	pressure
P^*	characteristic pressure
p_a	dimensionless pressure at the surface
P_a	pressure at the surface
P_{max}	maximum pressure at the surface
q_a	dimensionless heat flux at the surface
Q_a	heat flux at the surface
Q_{max}	maximum heat flux at the surface
T	temperature
T^*	characteristic temperature
T_l	liquidus temperature
T_s	solidus temperature
t_a	dimensionless gas shear stress at the surface
T_m	melting temperature
u	dimensionless velocity in x
U	velocity in X
U^*	characteristic velocity in X
u_m	dimensionless base material in x
U_m	base material velocity in X
U_∞	welding velocity
w	dimensionless velocity in z
W	velocity in Z
W^*	characteristic velocity in Z
w_m	dimensionless base material velocity in z
W_m	base material velocity in Z
z'_f	dimensionless free surface position
Z'_f	free surface position
z'_m	dimensionless melting interface position
Z'_m	melting interface position

Greek Symbols

α	liquid heat diffusivity
β	volumetric thermal expansion
δ^*	characteristic thickness of liquid film
Φ	electric potential
Φ^*	characteristic electric potential
φ	dimensionless electric potential
μ	viscosity
μ_0	magnetic permeability of vacuum
ν	kinematic viscosity
Π_i	Buckingham's dimensionless parameters
θ	dimensionless temperature
ρ	liquid density
σ	surface tension
σ_e	electrical conductivity
σ_T	surface tension temperature coefficient
τ_a	gas shear stress at the surface
τ_{max}	maximum gas shear stress at the surface
ω	angle between tangent of melting front and horizontal
ω_0	angle between secant of melting front and horizontal

Subscript

flat	corresponds to an arc on a flat surface

Superscript

*	unknown scaling parameter

References

1. T. Yamamoto and W. Shimada, presented at *International Symposium in Welding*, Osaka, Japan, 1975.
2. W. Shimada and S. Hoshinouchi, *Quart. J. Japan Weld. Soc.*, 51 (3), 280-286. (1982).
3. W.F. Savage, E.F. Nippes, and K. Agusa, *Weld. J.*, 212s-224s. (July 1979).
4. M.L. Lin and T.W. Eagar, *Weld. J.*, 163s-169s. (June 1985).
5. B.J. Bradstreet, *Weld. J.*, 314s-322s. (July 1968).
6. P.F. Mendez, Doctor of Philosophy, Massachusetts Institute of Technology, 1999.
7. K. Ishizaki, presented at *Physics of the Welding Arc*, London, UK, 1962.
8. K. Ishizaki, presented at *Weld Pool Chemistry and Metallurgy*, London, UK, 1980.
9. V.P. Demyantsevich and V.D. Matyukhin, *Svar. Proiz.*, (10), 1-3. (1972).
10. A. Matsunawa and K. Nishiguchi, presented at *Arc Physics and Weld Pool Behaviour*, London, UK, 1979.
11. R.T.C. Choo, J. Szekely, and R.C. Westhoff, *Weld. J.*, 69 (9), 346s-361s. (1990).
12. S.I. Rokhlin and A.C. Guu, *Weld. J.*, 381s-390s. (August 1993).
13. M.L. Lin and T.W. Eagar, presented at *Transport Phenomena in Materials Processing*, 1983.
14. G.M. Oreper and J. Szekely, *J. Fluid Mech.*, 147 53-79. (1984).
15. M.E. Thompson and J. Szekely, *Int. J. Heat Mass Transfer*, 32 (6), 1007-1019. (1989).
16. D. Rivas and S. Ostrach, *Int. J. Heat Mass Transfer*, 35 (6), 1469-1479. (1992).
17. P.S. Wei and W.H. Giedt, *Weld. J.*, 251s-259s. (September 1985).
18. N.-S. Tsai, *Heat Distribution and Weld Bead Geometry in Arc Welding*, Doctor of Philosophy, Massachusetts Institute of Technology, 1983.
19. R.T.C. Choo, *Mathematical Modelling of Heat and Fluid Flow Phenomena in a Mutually Coupled Welding Arc and Weld Pool*, Doctor of Science, Massachusetts Institute of Technology, 1991.
20. Omega Engineering Inc., *Chart of Dimensionless Numbers*, Poster, (1995).
21. U. Gratzke, P.D. Kapadia, J. Dowden, J. Kroos, and G. Simon, *J. Phys. D: Appl. Phys.*, 25 1640-1647. (1992).